Appl. Phys. A (2016) 122:107
DOI 10.1007/s00339-016-9625-6

Applied Physics A
Materials Science & Processing

INVITED PAPER

Ultrashort laser pulse ablation of copper, silicon and gelatin: effect of the pulse duration on the ablation thresholds and the incubation coefficients

Chandra S. R. Nathala[1,2] · Ali Ajami[1,3] · Wolfgang Husinsky[1] · Bilal Farooq[1] · Sergey I. Kudryashov[4,5] · Albena Daskalova[6] · Irina Bliznakova[6] · Andreas Assion[2]

Received: 18 October 2015 / Accepted: 11 January 2016 / Published online: 1 February 2016

Abstract In this paper, the influence of the pulse duration on the ablation threshold and the incubation coefficient was investigated for three different types of materials: metal (copper), semiconductor (silicon) and biopolymer (gelatin). Ablation threshold values and the incubation coefficients have been measured for multiple Ti:sapphire laser pulses (3 to 1000 pulses) and for four different pulse durations (10, 30, 250 and 550 fs). The ablation threshold fluence was determined by extrapolation of curves from squared crater diameter versus fluence plots. For copper and silicon, the experiments were conducted in vacuum and for gelatin in air. For all materials, the ablation threshold fluence increases with the pulse duration. For copper, the threshold increases as $\tau^{0.05}$, for silicon as $\tau^{0.12}$ and for gelatin as $\tau^{0.22}$. By extrapolating the curves of the threshold fluence versus number of pulses, the single-shot threshold fluence was determined for each sample. For 30 fs pulses, the single-shot threshold fluences were found to be 0.79, 0.35, and 0.99 J/cm^2 and the incubation coefficients were found to be 0.75, 0.83 and 0.68 for copper, silicon and gelatin, respectively.

✉ Wolfgang Husinsky
husinsky@iap.tuwien.ac.at

[1] IAP, Vienna University of Technology, Wiedner Hauptstrasse 8-10, 1040 Vienna, Austria

[2] Spectra-Physics Vienna, Fernkorngasse 10, 1100 Wien, Austria

[3] Faculty of Physics, Semnan University, Pardis 1, 19111-35131 Semnan, Iran

[4] ITMO University, Kronverkskiy prospect 49, St.-Petersburg 197101, Russia

[5] Lebedev Physical Institute, Leninskiy prospect 53, Moscow 119991, Russia

[6] Institute of Electronics, Bulgarian Academy of Sciences, 72, Tsarigradsko Chaussee blvd., 1784 Sofia, Bulgaria

1 Introduction

Ultrafast lasers have been of increasing interest in material processing applications due to their capability of precise micromachining of a large variety of materials: metals, semiconductors, polymers, dielectrics, biological materials, etc [1]. The processes that occur when a laser pulse irradiates a material can be divided into two domains: non-thermal domain (for processes that take place up to few ps) and thermal domain (for longer durations). The laser–matter interaction processes that happen with laser pulses of duration greater than characteristic electron-phonon relaxation times ($\tau_{ep} \sim 10$ ps) seems to have been fairly understood [2–4]. However, when an ultrashort laser pulse irradiates a material, the non-thermal processes that occur depend on the class of the material irradiated as well as the intensity of the irradiation. The precise processes and the sequence of processes that take place are far from understood [3, 5]. Laser ablation refers to as material removal from the surface of a medium by irradiating with laser pulses. Depending on the class of the material, different processes take place preceding laser ablation. For example, in metals which have abundant free elections, absorption creates hot electrons in a cold lattice and after electron-electron scattering, electron-phonon-scattering sets in, followed by melting, boiling and ablation. To a certain extent, these processes can be described by a two temperature model. In case of dielectrics and wide-bandgap semiconductors, absorption of radiation can be understood by multi-photon excitation and impact ionization with subsequent avalanche ionization. These carriers then thermalize

to a Fermi–Dirac distribution while transferring their excess energy to phonons. These phonons then recombine to a Bose–Einstein distribution and thermal processes follow. It is worth mentioning that upon irradiation with high peak intensities, dielectrics can exhibit metal-like properties. Hence, understanding the exact processes that take place upon femtosecond laser irradiation is a complex process involving linear and several nonlinear processes taking place simultaneously. Ablation threshold fluence, usually defined as the minimum laser fluence necessary to initiate the ablation process (material removal), is an important parameter which can give insight into the physical processes taking place in the material. Knowing the values is also necessary to deposit a defined amount of energy for precision material processing applications. The single-shot ablation threshold for ultrashort laser pulse ablation depends on the thermal and dynamical properties of the material. In multi-pulse regime, it is well established that the ablation threshold depends on the number of laser pulses exciting the same spot. The threshold fluence normally decreases with laser shot number [6, 7]. This phenomenon is referred to as material incubation, and the origin of the incubation is still under debate. The reduction in ablation threshold fluence follows a power law equation which holds for all materials [6, 8] and can be ascribed to higher energy coupling efficiency [9]. An increase in surface roughness after multi-shot irradiation due to ripples formation or accumulation of surface defects results in reduction in the reflectance [10] and thus leads to enhance the absorption and then a decrease in ablation threshold [11]. It has also been suggested that the incubation behaviour for metals can be due to the accumulation of plastic deformation resulting from laser-induced thermal stress fields [8]. The ablation threshold is usually determined by inspection of the exposed area with a microscope or by detecting changes in the scattering pattern produced by a probe laser or by detecting the ion emission using time-of-flight spectrometers [12]. In the most frequently used method to determine the ablation threshold, the squared crater diameter is plotted as a function of the pulse fluence (F). Linear extrapolation of the plot of the squared crater diameter versus ln (F) yields the ablation threshold. The advantage of this technique is that the measurements can be performed at fluences well above threshold for which the detected fingerprint signals are clearly detectable by far-field microscopy [7]. The actual physical mechanisms of laser ablation depend on the type of materials and the irradiation properties such as laser wavelength [10], pulse duration [13–19] and repetition rate [14, 20]. Change in the repetition rate affects the ablation threshold in two respects. Increasing the repetition rate, on the one hand, leads to particle shielding which reduces the absorption and thus limits the laser ablation efficiency. On the other hand, it leads to heat accumulation that causes melting. The latter, especially in case of metals with a relatively low thermal conductivity, prevents the high level of precision which is achievable at lower repetition rates. Using shorter pulses makes it possible to prevent heat accumulation arising from irradiating with high-repetition-rate laser pulses since for pulses of a few picoseconds or shorter, heat diffusion is frozen within the interaction volume and the shock-like energy deposition leads to ablation [18]. Nevertheless, as soon as the pulse energy is increased melting cannot be avoided in multi-pulses femtosecond laser ablation processes [20]. It has been observed that the damage threshold depends on the pulse duration. For long pulses (eg. $\tau > 10$ ps), where damage on the surface of a medium results from conventional heating and melting, the damage threshold scales as $\tau^{0.5}$ with pulse duration [21, 22]. However, a deviation from this scaling has been observed for shorter pulses where damage results from plasma formation and ablation [17, 22]. Although the ablation threshold in the short-pulse regime reduces with decreasing the pulse duration, this dependency is weaker than what is observed in the long-pulse regime. Till date, many authors have investigated the dependence of ablation threshold fluence on various laser parameters, but most studies were limited to a particular pulse duration or number of shots or material. A comprehensive study for different type of materials under identical experimental conditions was missing. In this paper, a systematic study was carried out to investigate the influence of pulse duration on the ablation thresholds and the incubation coefficients for three different types of materials: metal (copper), semiconductor (silicon) and biopolymer (gelatin) in 10–550 fs range. The results indicate that the threshold fluence reduces with decreasing the pulse duration. The dependence of the threshold fluence on the pulse duration was determined as $F_{\text{th}} \propto \tau^{0.05}$ for copper, $F_{\text{th}} \propto \tau^{0.12}$ for silicon and $F_{\text{th}} \propto \tau^{0.22}$ for gelatin.

2 Experiment

Three materials (copper, silicon and gelatin) were irradiated by a commercially available Ti:sapphire laser (Femtopower Compact PRO, Spectra-Physics Vienna) generating pulses centred at $\lambda \approx 800$ nm (the spectral full width at half maximum >40 nm) with maximum energy $E = 1$ mJ/pulse of $\tau = 30$ fs duration at repetition rate of $\nu = 1$ kHz. The copper sample used in these experiments is a mechanically polished 1-mm-thick foil (metal basis, 99.99 % purity, Alfa Aesar GmbH). The silicon sample used is a <100>-*N*-type, single-side polished-silicon wafer containing no dopants (Sigma-Aldrich). Gelatin films of 20 μm thickness used in the experiments were

prepared by dissolving 2.0 g of gelatin in 20 ml of distilled water, which was then heated up to 60 °C. The resulting viscous solution was shuffled for 35 min at this temperature to fully dissolve the gelatin. A thin layer of this solution was then applied on microscopic slides. The pulses were focused by a one-inch 90° off-axis parabolic mirror of focal length 150 mm on the target placed inside a small vacuum chamber which is mounted on a XYZ stage. The samples were irradiated at normal incidence and in stationary mode with different pulse energies, and number of pulses, for four different pulse durations (10, 30, 250 and 550 fs). Defined number of pulses (spaced 1 ms apart) are extracted by controlling the internal Pockels cell of the amplifier. The energy was varied by a half-wave plate and a polarizer unit placed before the compressor in the amplifier. Before each exposure, the pulse energy (E) was measured after the off-axis mirror, and before the entrance window of the vacuum chamber, by a pyroelectric detector (J-25MB-LE & J-10MB-LE, Coherent Inc.) and an energy meter (LabMax-TOP, Coherent Inc.). Standard deviation of pulse-to-pulse energy stability was determined to be 1.3 %. Post-experiment, the reflection losses at the input window of the chamber was measured and accounted for in the results presented here. The pulse duration was varied by changing the dispersive path length of the compressor in the amplifier. The 10 fs duration pulses (the spectral full width at tenth of maximum >300 nm) used in the experiments are generated by a hollow-core-fibre and compressor unit (Kaleidoscope, Spectra-Physics Vienna). The pulse duration was measured by a homemade background-free autocorrelator and commercially available autocorrelator (Femtometer, Spectra-Physics Vienna). Copper and silicon samples were irradiated in vacuum (10^{-3} mbar), and gelatin was irradiated in air as gelatin film was getting detached from the substrate when placed in the vacuum chamber. We preferred to conduct the experiments in vacuum to prevent the nonlinear effects, which could be significant for shorter pulse durations.

3 Results and discussions

When a laser beam is incident on a material surface, the ablation of the material occurs only when the incident laser pulse energy exceeds a minimum value called the ablation threshold. Ablation threshold values depend on several laser and material properties. For a laser beam having a Gaussian spatial distribution, for a given number of pulses (N), and pulse energy (E_p), the ablation crater diameter (D) formed on the material can be related to the ablation threshold, $F_{th}(N)$ [23] by

$$D^2 = 2w_0^2 \ln\left(\frac{F}{F_{th}(N)}\right), \quad (1)$$

where w_0 is the $1/e^2$ gaussian beam radius and F is the peak fluence given by,

$$F = \frac{2E_p}{\pi w_0^2} \quad (2)$$

As can be seen from Eq. (1), the squared ablation crater diameter goes linearly with the peak laser fluence (F), which is related to pulse energy E_p by Eq. (2). This makes it possible to determine the beam radius (w_0) from a plot of the squared crater diameters (D^2) versus the logarithm of the laser pulse energy (E_p). Figure 1 shows the craters formed on copper, silicon and gelatin when irradiated with femtosecond laser pulses. Once the spot size is known, the pulse energy values can be converted to the fluence using Eq. (2) and then the threshold fluence for each N ($F_{th}(N)$) of the material can be determined from the same plot by extrapolating the curve to the zero crater diameter. Figure 2 shows the squared crater diameter versus fluence for silicon when irradiated with 3, 10, 30, 100, 300 and 1000 pulses of 250 fs duration. For each shot-number, the squared crater diameter shows a linear behaviour versus the logarithm of the laser fluence from which the ablation fluence threshold can be determined. Data for other pulse durations of 10, 30 and 550 fs and for all three samples (i.e. 12 plots) were plotted (not shown here), and Figs. 3, 4 and 5 summarize the results for copper, silicon and gelatin, respectively. It can be seen from Fig. 3 that the ablation threshold decreases with increasing number of pulses. This reduction in threshold can be explained in terms of the incubation model [6]. The relation between single-shot threshold fluence $F_{th}(1)$ and N-shot threshold fluence $F_{th}(N)$ has been proposed as given by

$$F_{th}(N) = F_{th}(1)N^{S-1} \quad (3)$$

where S is called the incubation coefficient characteristic to the accumulation behaviour. $S = 1$ implies no incubation effect. A more elaborate model of incubation effect is given in [7]. It is clear that Eq. 3 can be valid only up to a certain number of pulses as the threshold fluence cannot reduce indefinitely. On the other hand, for lower N (1–10 pulses), the initial condition of the sample and the peak-to-peak pulse energy variation of the laser are critical for determining accurate values. For this reason, only the data points from $N = 10$ to 300 are used for fitting in the results presented here. The below subsections Sects. 3.1, 3.2 and 3.3 report the experimental conditions and results in detail for copper, silicon and gelatin, respectively. In Sect. 3.4, the dependence of the threshold fluence and the incubation coefficient on the pulse duration is reported.

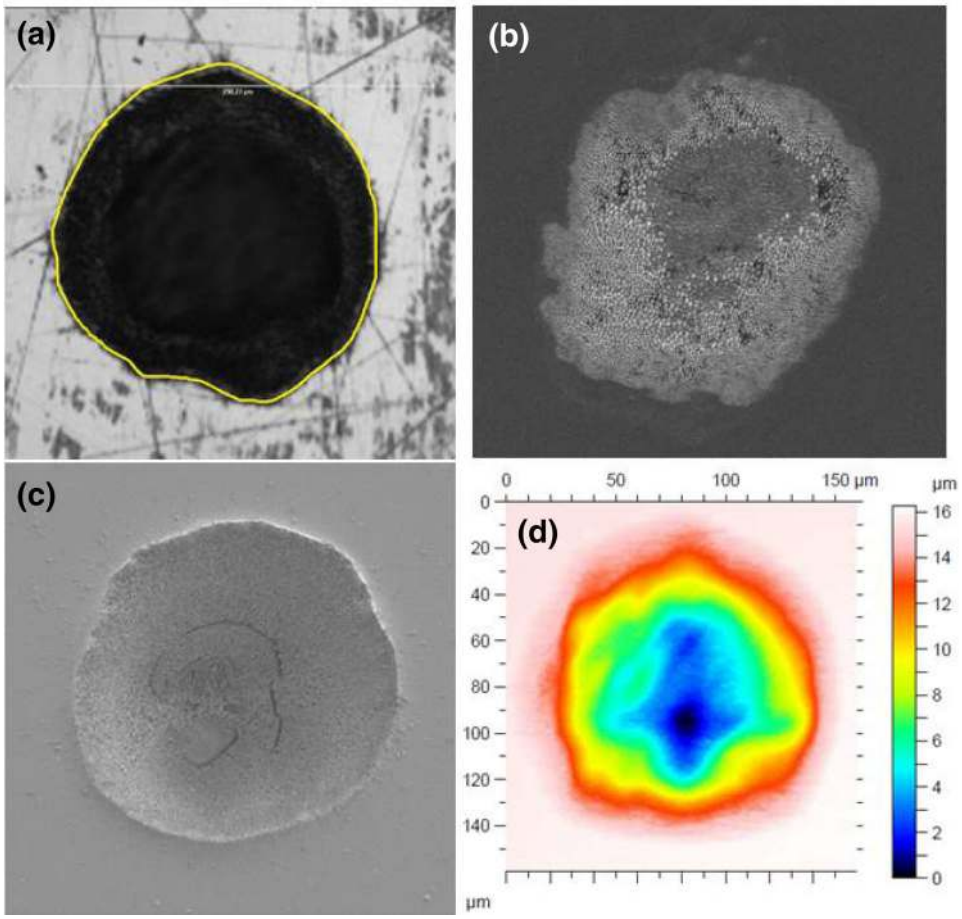

Fig. 1 **a** Optical microscope image of spot irradiated on copper sample with 300 pulses of 270 μJ energy and 550 fs duration. **b** SEM image of silicon sample irradiated with 100 pulses of 160 μJ and 30 fs. **C** Gelatin sample irradiated with 100 pulses of 100 μJ and 10 fs. **d** Confocal image of spot on copper sample after irradiating with 300 pulses of 180 μJ energy and 550 fs

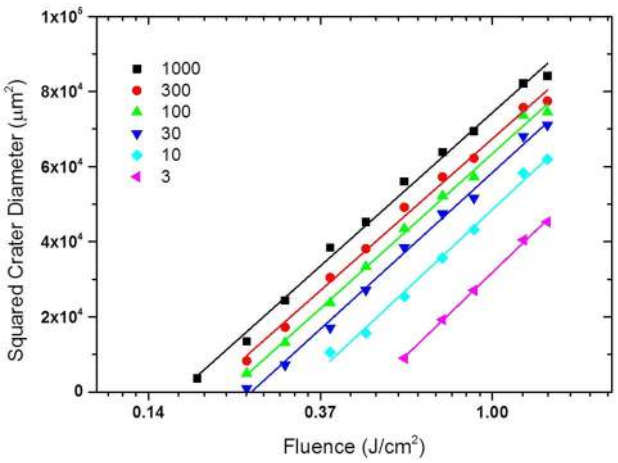

Fig. 2 Squared crater diameters versus the laser fluence for different number of applied laser pulses on a silicon sample when irradiated with 250 fs laser pulses

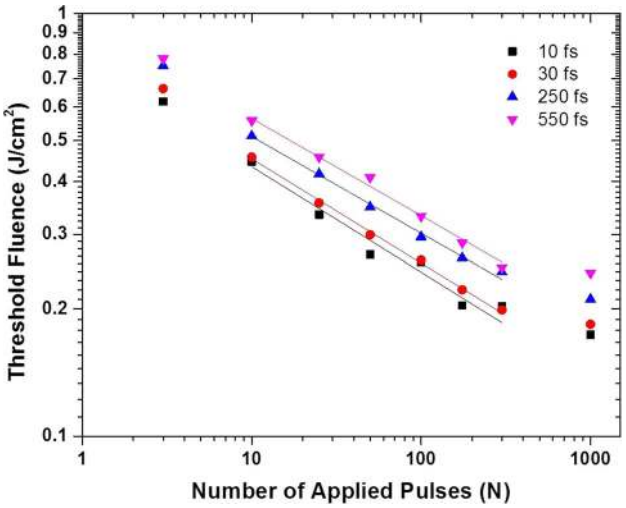

Fig. 3 Threshold fluence versus the number of applied pulses on a copper sample for four different pulse durations in vacuum. The *solid line* represents a least square fit using Eq. 3, from which $S = 0.75$, 0.76, 0.77, 0.77 were extracted for pulse durations 10, 30, 250 and 550 fs, respectively

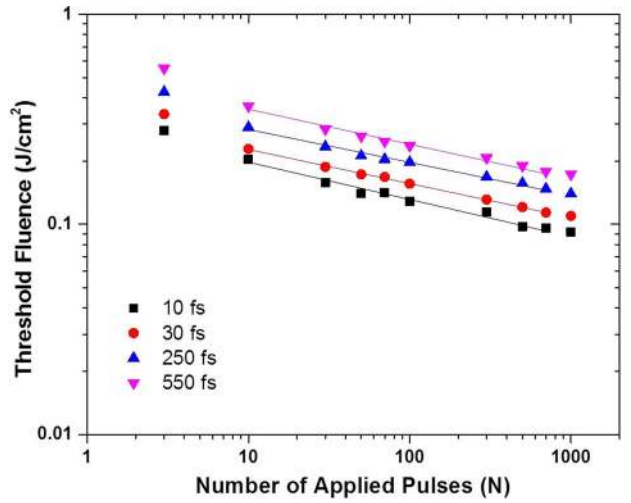

Fig. 4 Threshold fluence versus the number of applied pulses on a silicon sample for four different pulse durations in vacuum. The *solid line* represents a least square fit using Eq. 3, from which $S = 0.82$, 0.83, 0.84 and 0.84 were extracted for pulse durations 10, 30, 250 and 550 fs, respectively

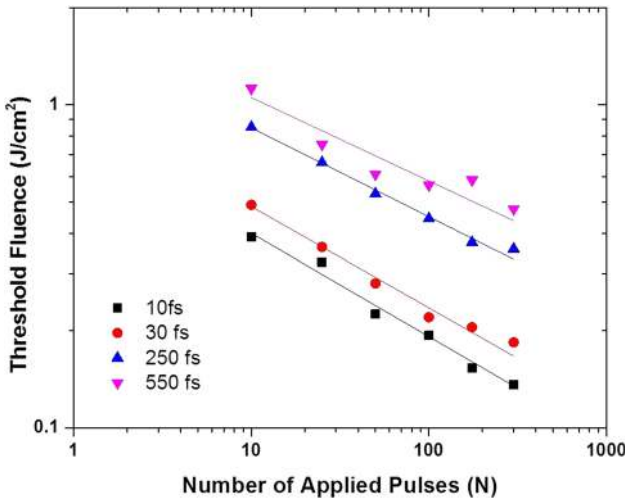

Fig. 5 Threshold fluence versus the number of applied pulses on a gelatin film for four different pulse durations in air. The *solid line* represents a least square fit using Eq. 3, from which $S = 0.68$, 0.69, 0.72 and 0.74 were extracted for pulse durations 10, 30, 250 and 550 fs, respectively

3.1 Copper

A copper sample was polished using a commercially available polishing machine (Allied High Tech Products Inc.) using sand paper up to 4000 grit and finally with 0.02-μm silica suspension. Mirror-like copper sample was then irradiated in vacuum with 3, 10, 25, 50, 100, 175, 300 and 1000 pulses with varying energy and for different pulse durations (10, 30, 250 and 550 fs). The irradiated spots were analysed with optical and confocal microscopes (Fig. 1a, d). Since the spots were not perfectly circular, the crater area (solid yellow line in Fig. 1a) was determined for each spot using ImageJ software and the squared crater diameter was determined by assuming it to be circular (equating it to area of a circle). Confocal images (Fig. 1d) were used to identify the ablation crater accurately. The squared crater diameter was plotted against the applied pulse energy for each N and corresponding w_0 value was determined from the slope of the linear fit curves. For best fits (R^2 value $\sim$99.7 %), the value of w_0 gradually increased from 63 to 72 μm as N increased from 3 to 1000. We observed this for all pulse durations and also for other metals (steel). However, for silicon it was not significant. This makes us to conclude that there could be other mechanisms responsible for higher crater diameters at higher F and N in metals. The energy values were then converted to fluence values, and the ablation threshold fluence was determined for each N by extrapolation. Table 1 shows the threshold values for different N and for all 4 pulse durations. The errors associated with the threshold fluence (about 10 %, not shown in the plots) arise from the error in determination of the spot size from the slope. Figure 3 shows the threshold fluence versus N for copper for different pulse durations. By fitting Eq. 3 to the data points, the single-shot threshold fluence $F_{th}(1)$ was extracted as 0.77, 0.79, 0.86 and 0.95 J/cm^2 and the incubation coefficient S as 0.75, 0.76, 0.77 and 0.77 for pulse durations 10, 30, 250 and 550 fs, respectively. The obtained ablation threshold values are slightly higher than that reported in [8] and lower than that reported in [9]. In both cases, the experiments were conducted in air, whereas we conducted our experiment in vacuum environment. To verify the reliability of the threshold values obtained in this experiment, the experiment was repeated for $N = 100$ at same focal position with an other sample polished on an other day and we observed an offset of about 15 % for all pulse durations, but the dependence on pulse duration showed similar behaviour. The variation of single-shot threshold fluence with pulse duration is discussed in Sect. 3.4.

3.2 Silicon

A silicon sample was irradiated in vacuum with 3, 10, 30, 50, 70, 100, 300, 500, 700 and 1000 pulses with varying energy and for different pulse durations (10, 30, 250 and 550 fs). The irradiated spots were analysed with SEM, and the ablation threshold fluence values were determined for each N by the procedure explained in Sect. 3.1. Table 2 shows the ablation threshold values for different N and for all 4 pulse durations. The errors associated with the threshold fluence (not shown in the plots) arising from error in spot size measurements is about 6 %. Figure 4 shows the threshold fluence versus N for different pulse durations. By fitting Eq. 3 to the data points, the single-shot

Table 1 Ablation threshold values of copper for different N in vacuum as determined by the diameter regression technique for 10, 30, 250 and 550 fs

Pulse duration (fs)	F_{th} (3)	F_{th} (10)	F_{th} (25)	F_{th} (50)	F_{th} (100)	F_{th} (175)	F_{th} (300)	F_{th} (1000)
10	0.619	0.446	0.334	0.269	0.258	0.204	0.203	0.174
30	0.664	0.457	0.356	0.299	0.261	0.222	0.199	0.184
250	0.752	0.513	0.417	0.348	0.296	0.264	0.245	0.211
550	0.781	0.557	0.457	0.409	0.331	0.286	0.251	0.243

The errors (about 10 %, not shown) arise from the error in determination of the spot size from the slope

Table 2 Ablation threshold values of silicon for different N in vacuum as determined by the diameter regression technique for 10, 30, 250 and 550 fs

Pulse duration (fs)	F_{th} (3)	F_{th} (10)	F_{th} (30)	F_{th} (50)	F_{th} (100)	F_{th} (300)	F_{th} (500)	F_{th} (1000)
10	0.279	0.203	0.158	0.139	0.129	0.114	0.097	0.092
30	0.334	0.228	0.187	0.172	0.155	0.131	0.120	0.109
250	0.427	0.290	0.234	0.212	0.198	0.168	0.157	0.140
550	0.552	0.365	0.283	0.262	0.236	0.207	0.190	0.173

The errors (about 6 %, not shown) arise from the error in determination of the spot size from the slope

Table 3 Ablation threshold values of 20-um gelatin film sample for different N in air as determined by the diameter regression technique for 10, 30, 250 and 550 fs

Pulse duration (fs)	F_{th} (10)	F_{th} (25)	F_{th} (50)	F_{th} (100)	F_{th} (175)	F_{th} (300)
10	0.390	0.326	0.225	0.193	0.153	0.136
30	0.490	0.363	0.280	0.220	0.205	0.184
250	0.853	0.663	0.530	0.444	0.375	0.358
550	1.125	0.755	0.610	0.564	0.585	0.476

The errors (about 7 %, not shown) arise from the error in determination of the spot size from the slope

threshold fluence F_{th} (1) was extracted as 0.297, 0.329, 0.405 and 0.518 J/cm^2 and the incubation coefficient S as 0.82, 0.83, 0.84 and 0.84 for pulse durations 10, 30, 250 and 550 fs, respectively. Bonse et al. have reported the dependence of threshold fluence on pulse duration of silicon for $N = 100$ pulses [13] and incubation coefficient as 0.84 with 130 fs pulses. Our results (see Tables 2, 3, 4) match very closely with their results. However, Bonse et al. conducted their experiments in air environment and we did in vacuum.

3.3 Gelatin

A gelatin film was irradiated with 10, 25, 50, 100, 175 and 300 pulses like as described in the previous sections and the ablation threshold fluence is determined. Table 3 shows the ablation threshold values for different N and for all 4 pulse durations. The errors associated with the threshold fluence (about 7 %, not shown in the plots) arise from the error in determination of the spot size from the slope. Figure 5 shows the plot of threshold fluence versus number of applied pulses for different pulse durations. As can be clearly seen from Fig. 5, the threshold fluence values are lower for shorter pulse durations for all N. The solid lines shows the fit curve using Eq. 3. From the fitting, the incubation coefficient S was determined as 0.68, 0.69, 0.72 and 0.74 for 10, 30, 250 and 550 fs, respectively, and by extrapolation of the fitted curve, single-shot threshold fluences were determined as 0.83, 0.99, 1.59 and 1.91 J/cm^2 for 10, 30, 250 and 550 fs, respectively. We observed that the threshold fluence depends on the concentration of the gelatin. In this experiment, we dissolved 2.0 g of gelatin in 20 ml of millipore water. When samples are prepared with 1.6 g of gelatin dissolved in 20 ml of water, we measured lower thresholds values, but the dependence on pulse duration was the same.

3.4 Pulse width dependence

Table 3 summarizes the results of the derived single-shot threshold fluences of copper, silicon and gelatin for 10, 30, 250 and 550 fs. The derived single-shot threshold fluence values are then plotted as a function of the pulse duration for all three materials and are shown in Fig. 6. It can be seen that the threshold fluence goes as $\tau^{0.05}$ for copper and as $\tau^{0.12}$ for

Table 4 Derived single-shot ablation threshold fluence and incubation coefficients for copper, silicon and 20-um-thick gelatin film sample for different pulse durations

Sample	F_{th} (1) (J/cm^2)				S				τ dep
	10 (fs)	30 (fs)	250 (fs)	550 (fs)	10 (fs)	30 (fs)	250 (fs)	550 (fs)	
Copper	0.77	0.79	0.86	0.95	0.75	0.76	0.77	0.77	$\tau^{0.05}$
Silicon	0.297	0.329	0.405	0.518	0.82	0.83	0.84	0.84	$\tau^{0.12}$
Gelatin	0.836	0.995	1.599	1.912	0.67	0.68	0.72	0.74	$\tau^{0.22}$

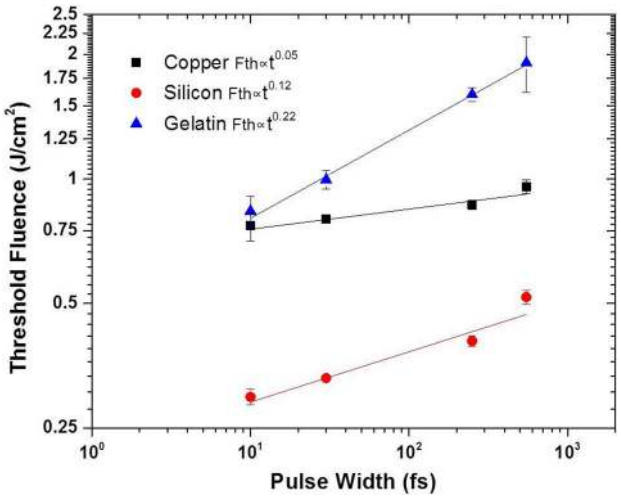

Fig. 6 Derived single-shot threshold fluence versus pulse width for copper, silicon and gelatin film samples

silicon and as $\tau^{0.22}$ for gelatin film. This general trend is consistent with multi-photon absorption as one of the underlying energy deposition mechanisms in these materials, with their power increasing from copper (linear intraband or two-photon interband absorption in near IR) to silicon (two-photon interband absorption in near IR) [24, 25] and 3–5 photons near-IR-photon absorption in gelatin. Since multi-photon absorption coefficient increases with increasing intensity, for the fixed laser fluence the threshold fluence decreases with the pulse width. As a result, the materials with higher powers of multi-photon absorption—transparent gelatin, to less extent, silicon—demonstrate the rising threshold fluence dependence on pulsewidth. In the case of copper, its negligible slope indicates that one-photon intraband IR absorption as the predominating absorption mechanism. Nevertheless though the dependence is small, a noticeable dependence on pulse duration was observed in our systematic multi-shot irradiation experiment.

4 Conclusions

In this contribution, the dependence of ablation threshold as well as incubation coefficient on pulse duration in the range of 10–550 fs has been systematically investigated for three different types of materials: metal (copper), semiconductor (silicon) and biopolymer (gelatin). Ablation threshold fluence values for multiple pulse irradiation ranging from 3 to 1000 has been reported. The ablation threshold for all investigated samples showed a decrease with pulse duration. For copper, the threshold scales as $\tau^{0.05}$, for silicon as $\tau^{0.12}$ and for gelatin as $\tau^{0.22}$. The incubation coefficient of gelatin showed a clear reduction at shorter pulse durations indicating higher incubation effect at shorter pulse durations. For copper and silicon, the incubation coefficient is nearly constant.

Acknowledgments Open access funding provided by TU WIen (TUW). This work was supported by the Österreichische Forschungsfdergesellschaft (FFG) (Project 834325). The SEM measurements were carried out using facilities at the University Service Centre for Transmission Electron Microscopy, Vienna University of Technology, Austria.

References

1. J. Cheng, C. Sheng Liu, S. Shang, D. Liu, W. Perrie, G. Dearden, K. Watkins, Opt. Laser Technol. **46**, 88 (2013)
2. J. Reif, Springer Ser. Mater. Sci. **191**, 29 (2014)
3. J. Reif, in *Laser-Surface Interactions for New Materials Production*, ed. by A. Miotello, P.M. Ossi (Springer, Berlin Heidelberg, 2010), p. 19
4. K.H. Leitz, B. Redlingshfer, Y. Reg, A. Otto, M. Schmidt, Phys. Proc. **12**, 230 (2011)
5. W. Kautek, O. Armbruster, Springer Ser. Mater. Sci. **191**, 42 (2014)
6. Y. Jee, M.F. Becker, R.M. Walser, J. Opt. Soc. Am. B **5**(3), 648 (1988)
7. Z. Sun, M. Lenzner, W. Rudolph, J. Appl. Phys. **117**(7), 073102 (2015)
8. P. Mannion, J. Magee, E. Coyne, G.O. Connor, T. Glynn, Appl. Surf. Sci. **233**(14), 275 (2004)
9. J. Byskov-Nielsen, J.M. Savolainen, M. Christensen, P. Balling, Appl. Phys. A **101**(1), 97 (2010)
10. C. McDaniel, A. Flanagan, G.M.O. Connor, Appl. Surf. Sci. **295**, 1 (2014)
11. B. Neuenschwander, B. Jaeggi, M. Schmid, A. Dommann, A. Neels, T. Bandi, G. Hennig, Proc. SPIE **8607**, 86070D (2013)
12. M. Hashida, S. Namba, K. Okamuro, S. Tokita, S. Sakabe, Phys. Rev. B **81**, 115442 (2010)

13. J. Bonse, S. Baudach, J. Krger, W. Kautek, M. Lenzner, Appl. Phys. A **74**(1), 19 (2002)
14. F.D. Niso, C. Gaudiuso, T. Sibillano, F. Mezzapesa, A. Ancona, P. Lugar, Phys. Proc. **41**, 698 (2013)
15. H.O. Jeschke, M.E. Garcia, M. Lenzner, J. Bonse, J. Krger, W. Kautek, Appl. Surf. Sci. **197–198**, 839 (2002)
16. H.O. Jeschke, M.E. Garcia, Appl. Surf. Sci. **197–198**, 107 (2002)
17. B.C. Stuart, M.D. Feit, S. Herman, A.M. Rubenchik, B.W. Shore, M.D. Perry, J. Opt. Soc. Am. B **13**(2), 459 (1996)
18. M. Lenzner, J. Krüger, S. Sartania, Z. Cheng, C. Spielmann, G. Mourou, W. Kautek, F. Krausz, Phys. Rev. Lett. **80**, 4076 (1998)
19. I. Artyukov, D. Zayarniy, A. Ionin, S. Kudryashov, S. Makarov, P. Saltuganov, JETP Lett. **99**(1), 51 (2014)
20. F.D. Niso, C. Gaudiuso, T. Sibillano, F.P. Mezzapesa, A. Ancona, P.M. Lugarà, Opt. Express **22**(10), 12200 (2014)
21. J. Byskov-Nielsen, J.M. Savolainen, M. Christensen, P. Balling, Appl. Phys. A **103**(2), 447 (2011)
22. B.C. Stuart, M.D. Feit, A.M. Rubenchik, B.W. Shore, M.D. Perry, Phys. Rev. Lett. **74**, 2248 (1995)
23. J.M. Liu, Opt. Lett. **7**(5), 196 (1982)
24. A. Ionin, S. Kudryashov, L. Seleznev, D. Sinitsyn, A. Bunkin, V. Lednev, S. Pershin, J. Exp. Theor. Phys. **116**(3), 347 (2013)
25. P. Danilov, A. Ionin, S. Kudryashov, S. Makarov, A. Rudenko, P. Saltuganov, L. Seleznev, V. Yurovskikh, D. Zayarny, T. Apostolova, J. Exp. Theor. Phys. **120**(6), 946 (2015)